Monthly Notices
of the
ROYAL ASTRONOMICAL SOCIETY

MNRAS **470,** 1960–1970 (2017) doi:10.1093/mnras/stx1341

Structure of accretion flows in nova-like cataclysmic variables: RW Sextantis and 1RXS J064434.5+334451

M. S. Hernandez,[1,2] S. Zharikov,[1⋆] V. Neustroev[3,4] and G. Tovmassian[1]

[1]*Instituto de Astronomía, Universidad Nacional Autónoma de México, Apdo. Postal 877, Ensenada, Baja California, Mexico, 22800*
[2]*Instituto de Física y Astronomía, Facultad de Ciencias, Universidad de Valparaíso, Av. Gran Bretaña 1111 Valparaíso, Chile*
[3]*Finnish Centre for Astronomy with ESO (FINCA), University of Turku, Väisäläntie 20, FI-21500 Piikkiö, Finland*
[4]*Astronomy Research Unit, PO Box 3000, FI-90014 University of Oulu, Finland*

Accepted 2017 May 26. Received 2017 May 17; in original form 2017 March 22

ABSTRACT

New time-resolved optical spectroscopic echelle observations of the nova-like cataclysmic variable RW Sextantis were obtained, with the aim of studying the properties of emission features in the system. The profile of the Hα emission line can be clearly divided into two ('narrow' and 'wide') components. Similar emission profiles are observed in another nova-like system, 1RXS J064434.5+33445, for which we also reanalysed the spectral data and redetermined the system parameters. The source of the 'narrow', low-velocity component is the irradiated face of the secondary star. We disentangled and removed the 'narrow' component from the Hα profile to study the origin and structure of the region emitting the wide component. We found that the 'wide' component is not related to the white dwarf or the wind from the central part of the accretion disc, but is emanated from the outer side of the disc. Inspection of literature on similar systems indicates that this feature is common for some other long-period nova-like variables. We propose that the source of the 'wide' component is an extended, low-velocity region in the outskirts of the opposite side of the accretion disc, with respect to the collision point of the accretion stream and the disc.

Key words: binaries: close – binaries: spectroscopic – stars: individual: RW Sextantis – stars: individual: 1RXS J064434.5+334451 – novae, cataclysmic variables.

1 INTRODUCTION

Cataclysmic variables (CVs) are interacting binaries comprised of a white dwarf (WD) as the primary and a late-type (K–M type) main-sequence star or a brown dwarf as the secondary (Warner 1995). The secondary star fills its Roche lobe and loses matter via the inner Lagrangian point L_1. Infalling matter forms an accretion disc around the WD unless its magnetic field is strong enough to prevent this. In CVs with low mass-transfer rates $\dot{M} < 10^{-9}$ M$_\odot$, known as dwarf novae (DNe), the accretion disc is usually in the low temperature and surface density state (quiescence). Every once in a while, the accretion disc builds up by increasing both the temperature and the surface density reaching thermal instability, which results in regular outbursts. Nova-like variables (NLs) in contrast to DNe are CVs that do not display such eruptive activity. The mass-transfer rate in NLs is estimated to be $\dot{M} \gtrsim 10^{-9}$ M$_\odot$ (Warner 1995), which allows their discs to remain in a high state most of the time. Spectrally, they resemble DNe in outbursts. They are found to have orbital periods longer than $\gtrsim$2 h. Historically, NLs that do not exhibit magnetic characteristics are also called UX UMa-type stars.

The optical spectra of NLs have a blue continuum and show a wide range of appearances, from pure absorption-line spectra to pure emission-line spectra. In some objects, the emission lines are embedded in broad absorption troughs. A typical NL spectrum usually shows a set of Balmer, He I and He II lines, and also the Bowen blend of fluorescence lines and weak absorption lines of metals. The profiles of emission lines in the optical range are usually single-peaked regardless of the system's inclination. This is in contrast to DNe, where emission lines are practically always double-peaked in high-inclination systems. The UV spectra of NLs exhibit P Cygni profiles of emission lines, implying the presence of a strong high-velocity wind (∼3000 km s^{-1}; see, e.g. Noebauer et al. 2010) in the inner part of the accretion disc.

Many NLs show long-term brightness variations on different time-scales. The most outstanding behaviour is observed in VY Scl stars (or 'anti-dwarf novae'), whose light curves display occasional, unpredictable low states of ∼1–6 mag for several weeks or even years. There is also another large group of systems, called SW Sex stars (Thorstensen, Davis & Ringwald 1991), which is distinguished from the rest of NLs by common properties. The SW Sex

⋆ E-mail: zhar@astrosen.unam.mx

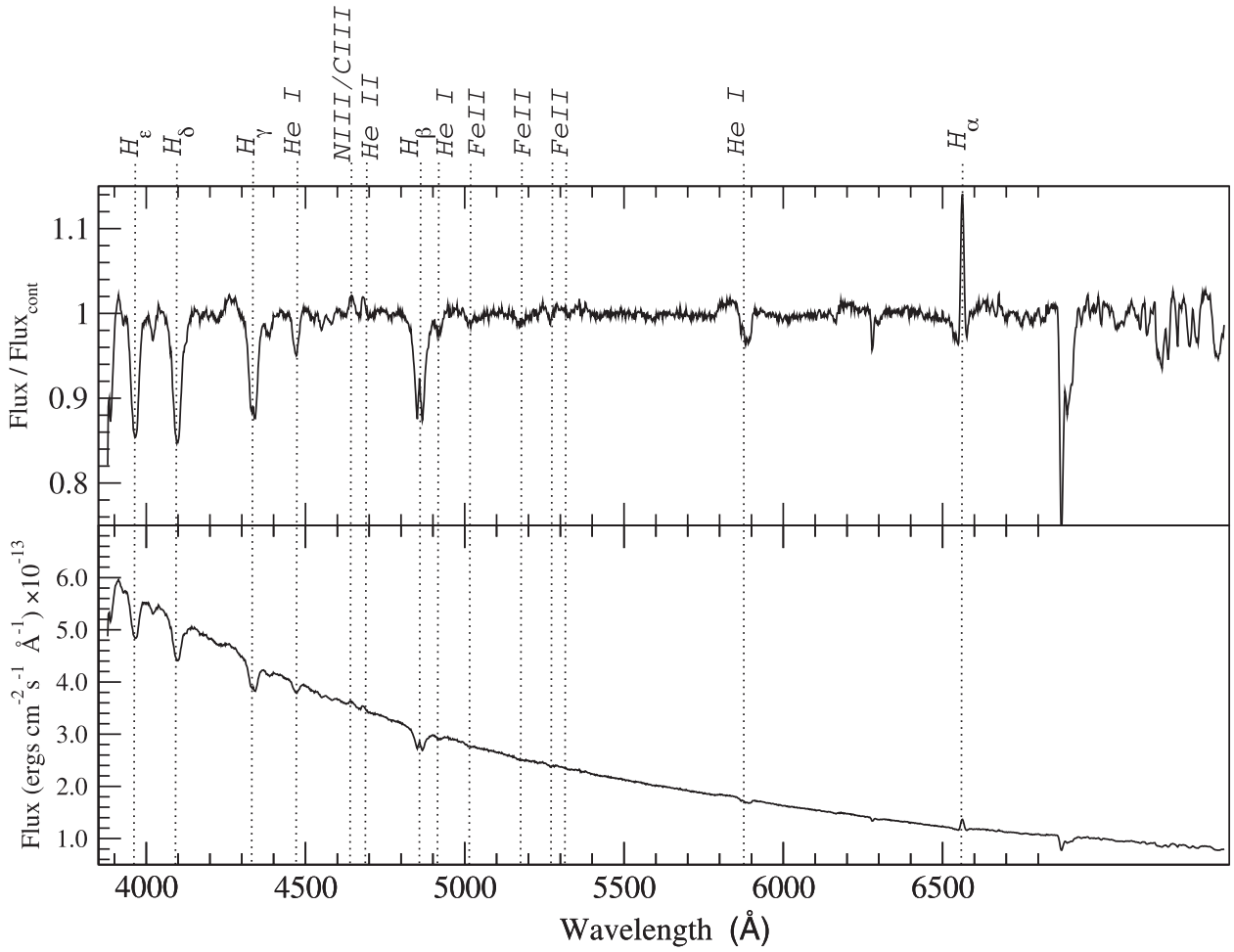

Figure 1. Flux-calibrated (bottom) and continuum-normalized (top) medium-resolution spectra of RW Sex. The spectral features are marked.

stars are mostly concentrated in the ∼3–4 h orbital period range. Most of them are deeply eclipsing systems, showing odd V-shaped eclipse profiles and simple single-peaked emission lines. They also show a distinct phase shift between the eclipse and the zero phase of the radial-velocity curve, high-velocity emission S-waves with maximum blueshift near phase ∼0.5 and transient absorption dips in the emission lines around phase 0.4–0.7.

In order to explain the appearance of single-peaked emission-line profiles in high-inclination CVs, a number of mechanisms have been widely discussed in the literature (see, e.g. Dhillon, Marsh & Jones 1997). In this paper, we make a new attempt to probe the formation of such lines, based on the high-resolution spectroscopy of two long-period NLs, RW Sextantis and 1RXS J064434.5+334451, for which hints of a multicomponent structure of emission lines in low-resolution spectra have been reported.

RW Sex is a relatively bright CV ($V \sim 10.6$ mag) with an orbital period of $P_{\rm orb} = 0.24507$ d (Beuermann, Stasiewski & Schwope 1992). The optical spectrum of RW Sex shows broad Balmer absorption lines with multicomponent emission cores, and weak He II and C III/N III emission lines (see Fig. 1). Based on phase-resolved spectroscopy, Beuermann et al. (1992) provided estimates of the RW Sex component masses and the orbital inclination: $M_1 = 0.84\ {\rm M}_\odot$, $M_2 = 0.62\ {\rm M}_\odot$, $i = 34^\circ \pm 6$, and the mass ratio $q \equiv M_2/M_1 = 0.74$. They also estimated the distance to the system of 150 pc. This is inconsistent with the Hipparcos parallax of 3.46±2.44 mas (Perryman et al. 1997), which corresponds to a distance of 289^{+689}_{-119} pc. The mass-transfer rate is estimated at $\dot{M} = (0.3 - 1.0) \times 10^{-8}\ {\rm M}_\odot\ {\rm yr}^{-1}$ (Linnell et al. 2010; Vitello & Shlosman 1993; Greenstein & Oke 1982). Ultraviolet observations show P Cyg profiles of emission lines (Greenstein & Oke 1982; Prinja et al. 2003), indicating the presence of a hot, fast (up to 4500 km s^{-1}) wind from the innermost portions of the disc. Linnell et al. (2010) analysed *Far Ultraviolet Spectroscopic Explorer*, *Hubble Space Telescope* and *International Ultraviolet Explorer* spectra of RW Sex and found the following system parameters: $M_1 = 0.9\ {\rm M}_\odot$, $M_2 = 0.67\ {\rm M}_\odot$, $\dot{M} = 2.0 \times 10^{-9}\ {\rm M}_\odot\ {\rm yr}^{-1}$, $i = 34^\circ$, $T_{\rm WD} = 50\,000$ K. Coppejans et al. (2015) reported the Very Large Array radio detection of RW Sex. The object showed non-variable flux of ∼33.6 μJy beam^{-1} in the range of 4226–8096 MHz with a spectral index of $\alpha = -0.5 \pm 0.7$ ($F = \nu^\alpha$), and probably of non-thermal origin. A compilation of available infrared data from the Two-Micron All-Sky Survey, *Spitzer* and the *Wide-field Infrared Survey Explorer* was reported by Hoard et al. (2014), who discussed the possible origin of the infrared excess in terms of emission from bremsstrahlung or circumbinary dust, with either mechanism facilitated by the mass outflows (e.g. disc wind/corona, accretion stream overflow, etc.) presented in NLs.

1RXS J064434.5+334451 ($V \sim 13.3$ mag) was discovered by Woźniak et al. (2004) in the Northern Sky Variability Survey. Sing et al. (2007) reported this object as a deep eclipsing CV with the orbital period of $P_{\rm orb} = 0.26937$d and derived the physical parameters of the system, such as the WD mass $M_1 = 0.66\ {\rm M}_\odot$, the mass ratio $q = 0.78$ and the WD temperature $T_{\rm WD} \sim 25\,000$ K. They classified

the system as a NL CV of the UX UMa-type or the SW Sex-type. Hernández Santisteban (2012), Echevarria (2015) and Hernández Santisteban et al. (2017) recently reported new time-resolved photometry and echelle spectroscopy of 1RXS J064434.5+334451. They constructed Doppler maps of the system in the Hα, Hβ, and He II 4686 emission lines and refined system parameters based on the obtained data. The WD with $M_1 = 0.82 \pm 0.06$ M$_\odot$ and the mass ratio $q = 0.96 \pm 0.05$ was proposed, assuming the system inclination of $i = 78^\circ \pm 2$ in Hernández Santisteban et al. (2017), which disagrees with Sing et al. (2007) and their own recent estimations: $M_1 = 0.91 \pm 0.04$ M$_\odot$, $q = 0.91 \pm 0.09$ from Hernández Santisteban (2012) and $M_1 = 0.76 \pm 0.04$ M$_\odot$, $q = 0.75 \pm 0.1$ from Echevarria (2015).

Regardless of different inclination angles, the Doppler maps of Balmer lines of 1RXS J064434.5+334451 and RW Sex are very similar. The Hα profile appears to have multiple but identical components in both objects. Therefore, we analysed the profiles of intense emission lines of both objects side by side in order to understand the origin and the sources of their constituent components. Moreover, we also redetermined the system parameters of 1RXS J064434.5+334451 based on the available time-resolved photometry and eclipse profile fitting. In this study, we used new observations of RW Sex and the original data of 1RXS J064434.5+334451 obtained and kindly provided by Hernández Santisteban et al.

This paper is structured as follows. In Section 2, we describe our spectroscopic observations of RW Sex and the corresponding data reduction. In Section 3, we present an analysis of emission-line profile components based on Doppler tomography of RW Sex. In Section 4, we revisit 1RXS J064434.5+334451 to determine the system parameters and to reanalyse its Doppler maps. The general discussion of obtained results and their application to NL systems of similar orbital periods follows in Section 5. Our conclusions are presented in Section 6.

2 OBSERVATIONS AND DATA REDUCTION

The spectroscopic data of RW Sex were obtained using the echelle REOSC spectrograph (Levine & Chakarabarty 1995) attached to the 2.1-m telescope of the Observatorio Astronómico Nacional at San Pedro Mártir (OAN SPM),[1] Mexico. The echelle spectrograph provides spectra spread over 27 orders, covering the spectral range ~3500–7105 Å with the spectral resolving power of $R \approx 18\,000$. A total of 73 echelle spectra were obtained during seven consecutive nights in 2015 and 36 spectra in 2016. A Tr–Ar lamp was used for wavelength calibration. The spectra were reduced using the `echelle` package in IRAF.[2] The medium resolution (~1.15 Åpix^{-1}) spectra were obtained using the same 2.1-m telescope and the Boller and Chivens (B&Ch) spectrograph. Standard procedures, including bias and flat-field correction, cosmic ray removal, wavelength and flux calibration were applied using the corresponding tasks in IRAF. The log of observations is given in Table 1.

Spectra of 1RXS J064434.5+334451 were obtained by Hernández Santisteban (2012) and Hernández Santisteban et al. (2017) using the same instrument/telescope set-up as in the case of RW Sex, at the same observatory. Moreover, they obtained the time-resolved photometry of the object with the 1.5-m telescope also located at OAN SPM. A full description of those observations and data reduction has been presented in previously cited publications. Only the Hα order of echelle spectra was used in our following analyses.

Table 1. Log of RW Sex spectroscopic observations. Echelle denotes the REOSC echelle spectrograph and B&Ch denotes the long-slit Boller and Chivens spectrograph.

Date (yyyy/mm/dd)	HJD start +245 0000	No. of exp.	Exposure (s)	Duration (h)
Echelle				
2015/01/13	7036.03109	3	900–1200	0.9
2015/01/14	7036.83745	10	900	2.5
2015/01/15	7037.83663	10	900–1200	2.8
2015/01/16	7039.00118	6	900	1.5
2015/01/17	7039.79971	15	900	3.7
2015/01/18	7040.79247	15	900	3.7
2015/01/19	7041.79253	14	900	3.5
2016/03/23	7470.83605	3	1200	1.0
2016/03/24	7471.78651	6	1200	2.0
2016/03/25	7472.77510	7	1200	2.3
2016/03/26	7473.80031	6	1200	2.0
2016/03/27	7474.77762	6	1200	2.0
2016/03/27	7475.78476	8	1200	2.7
B&Ch				
2016/01/19	7406.85160	1	1200	0.33
2016/01/18	7407.87406	2	1200	0.66
2016/02/10	7428.79462	20	300	1.65
2016/03/30	7477.64920	31	900	5.7

3 THE SPECTRUM, BALMER EMISSION LINES AND DOPPLER TOMOGRAPHY OF RW SEX

Fig. 1 shows the medium-resolution spectrum of RW Sex. The spectrum has strong broad Balmer absorption lines with multicomponent emission cores that are clearly visible in Hα and partly visible in Hβ, and there is a hint of emission in Hγ. Higher Balmer series lines show only absorption profiles. There are also He I 4026, 4144, 4388, 4471, 4922, 5015, 5876 and very weak Fe II 5169, 5276, 5316 absorption/emission lines. The high-excitation lines of He II 4686 and the C III/N III 4634–4651 blend are detected in emission. Also, the spectrum shows a relatively strong emission bump centred at ~5830 Å, which is probably a blend of C III 5827 and the C IV lines at 5801 and 5812 Å, and possibly of other highly excited lines blueward of He I 5876. These lines are very uncommon for CV spectra, and their detection in this wavelength region has been reported only for a few CVs (see, e.g. Neustroev et al. 2017). The continuum in a wide optical range can be described by a power law $F_\lambda \sim \lambda^\alpha$, where $\alpha = -3.08 \pm 0.01$ is steeper than $\alpha_{st} = -2.33$ adopted for the standard disc model (Lynden-Bell 1969).

Fig. 2 shows an example of a high-resolution ($R \approx 18\,000$) profile of the emission core of Hα. The profile has a complex structure consisting of at least two distinct variable components, which are clearly visible in trailed spectra of Hα and Hβ (Fig. 3, left-hand panels). One of these components looks strong and narrow, and it exhibits low-amplitude radial-velocity variations ($\lesssim$100 km s^{-1}), while the other seems weaker and wider and shows significantly larger radial-velocity variability (≈200–250 km s^{-1}).

We used Doppler tomography (Marsh & Horne 1988) to map the Hα and Hβ lines using our high-spectral-resolution observations (Fig. 3, two upper rows). The orbital zero phase was selected

[1] http://www.astrossp.unam.mx

[2] IRAF is distributed by the National Optical Astronomy Observatories, which are operated by the Association of Universities for Research in Astronomy, Inc., under cooperative agreement with the National Science Foundation.

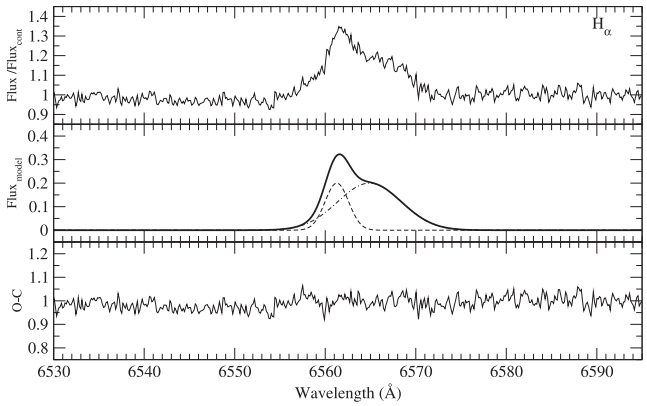

Figure 2. An example of the high-resolution H α profile of RW Sex (top panel), the result of a double-Gaussian fit to the profile (middle panel) and the residuals between the observed and calculated profiles (bottom panel). The underlying broad absorption component was removed by continuum normalization.

following the interpretation of Beuermann et al. (1992) that the narrow component of H α is a 'chromospheric' emission from the irradiated hemisphere of the secondary facing the accretion disc. It corresponds to the strongly concentrated emission inside the Roche lobe of the secondary star on the Doppler maps. In addition, the maps show a sign of an extended emission area on the bottom of the tomograms. This area corresponds to the 'wide' component of emission lines.

In order to study the structure of the wide emission component, we fitted the H α profiles with a sum of two Gaussians, denoted here as 'narrow' and 'wide'. They are characterized by the peak intensity I and the full width at half-maximum (FWHM), and their radial velocities depend on the orbital phase

$$v = \gamma - A \times \sin[2\pi(\varphi - \varphi_0)], \quad (1)$$

where γ is the systemic velocity, A is the semi-amplitude of the radial-velocity variation and φ is the orbital phase calculated relative to epoch $T_0 =$ HJD 245 7036.83486. Phase zero φ_0 is defined by the blue-to-red crossing of the corresponding emission component. The narrow Gaussian was fitted to the H α profile in individual spectra wherever it was feasible because at some phases the 'narrow' and 'wide' components are indistinguishable. The mean parameters of both the Gaussian components were deduced as the average of individual fits, and these are presented in Table 2. We then subtracted the average 'narrow' component from the observed profiles and calculated the Doppler map of the 'wide' component (Fig. 3, bottom panels). The tomogram does not show the usual 'doughnut' structure commonly observed from accretion discs. There is also no evidence for the gas stream/disc impact region emission. Instead, it displays an extended, asymmetric region of emission, mostly concentrated in the bottom half of the map in its lower-right quadrant. The brightest area is located far from the position of the WD ($V_x = 0$, $V_y \approx -100$ km s^{-1}), but does not extend beyond $\sim$300 km s^{-1} on the Doppler map. This is less than the minimal possible Keplerian velocity of the accretion disc with the largest, tidally truncated radius, which can be estimated using equation (2.61) from Warner (1995)

$$r_{\rm d}(\max) = a\frac{0.6}{1+q}, \quad (2)$$

where a is the binary separation and q is the mass ratio. For the adopted system parameters of RW Sex ($M_1 = 0.84$ M$_\odot$, $i = 34^\circ$, $q = 0.74$), the minimal Keplerian velocity of the largest disc is about 250 km s^{-1}, denoted in Doppler maps by the circle. Because the Keplerian velocity inside of the disc is higher than at the tidal limitation radius, the accretion disc in Doppler maps must always be located outside of the circle. However, one can clearly see that the emission from the 'wide' component is concentrated outside the accretion disc.

The tomograms also show another emission region centred at ($V_x = 100$ km s^{-1}, $V_y \approx 350$ km s^{-1}). After the removal of the 'narrow' component, this additional, 'third' component is visible more clearly in the trailed spectra and on the Doppler map. It might be associated with a low contrast spiral tidal shock in the outer parts of the accretion disc (Matsuda et al. 1990; Steeghs 2001; Kononov et al. 2012).

We also explored the Fe II 5316 line (Fig. 4). It is centrally placed in an echelle order and hence secures a better signal-to-noise ratio (S/N $\approx$ 60) at the continuum level than other Fe II lines detected in the spectra. In the summed spectrum, the line shows a broad absorption profile with a relatively strong emission core (Fig. 4, bottom panel). Although the line is noisy in individual spectra, it is easily traced in the trailed spectrum (Fig. 4, top-left panel), allowing us to construct a decent Doppler map (Fig. 4, top-right panel). The tomogram shows that the emission component emanates from the same source as the 'narrow' emission component of H α, which we identify as the heated face of the secondary star. The absorption component seems to originate in the accretion disc, close to the WD.

4 REVISITING 1RXS J064434.5+334451

The orbital periods of 1RXS J064434.5+334451 (0.2694d) and RW Sex (0.2451d) are very close and the Doppler mapping analysis of the Balmer lines showed remarkably similar structures of accretion flows in both systems. An additional advantage of 1RXS J064434.5+334451, compared with RW Sex, is the high inclination of the system with a prominent eclipse. This allows us to determine exactly the phase 0.0 of the system and to make an effort to identify the definite locations of emission-line sources. However, as we already noted, the system parameters determined by Sing et al. (2007), Hernández Santisteban (2012), Echevarria (2015) and Hernández Santisteban et al. (2017) for 1RXS J064434.5+334451 do not agree. Moreover, we note that the system parameters of Hernández Santisteban (2012) and Hernández Santisteban et al. (2017) do not seem realistic because a secondary star with a mass of $M_2 \geq 0.79$ M$_\odot$, as follows from their measurements, noticeably exceeds its Roche lobe for the given orbital period, regardless of whether it is on the main sequence or evolved.[3] This makes it difficult to determine the whereabouts of the sources of emission components. Therefore, in Section 4.1, we use another approach to improve the system parameters. Unlike the previous attempts, where only the dynamical constraints were considered, we rely on the eclipse profile at the same time as radial velocities. We fitted the combined V-band light curve of 1RXS J064434.5+334451 using the same eclipse modelling technique as in Zharikov et al. (2013) and Tovmassian et al. (2014). Additionally, in Section 4.2 we also reanalysed spectral data from Hernández Santisteban (2012) and Hernández Santisteban et al. (2017) with the using newly defined system parameters to determine the location of the 'wide' emission component source in 1RXS J064434.5+334451.

[3] See the empirical radius–period relationship (2.101) of Warner (1995).

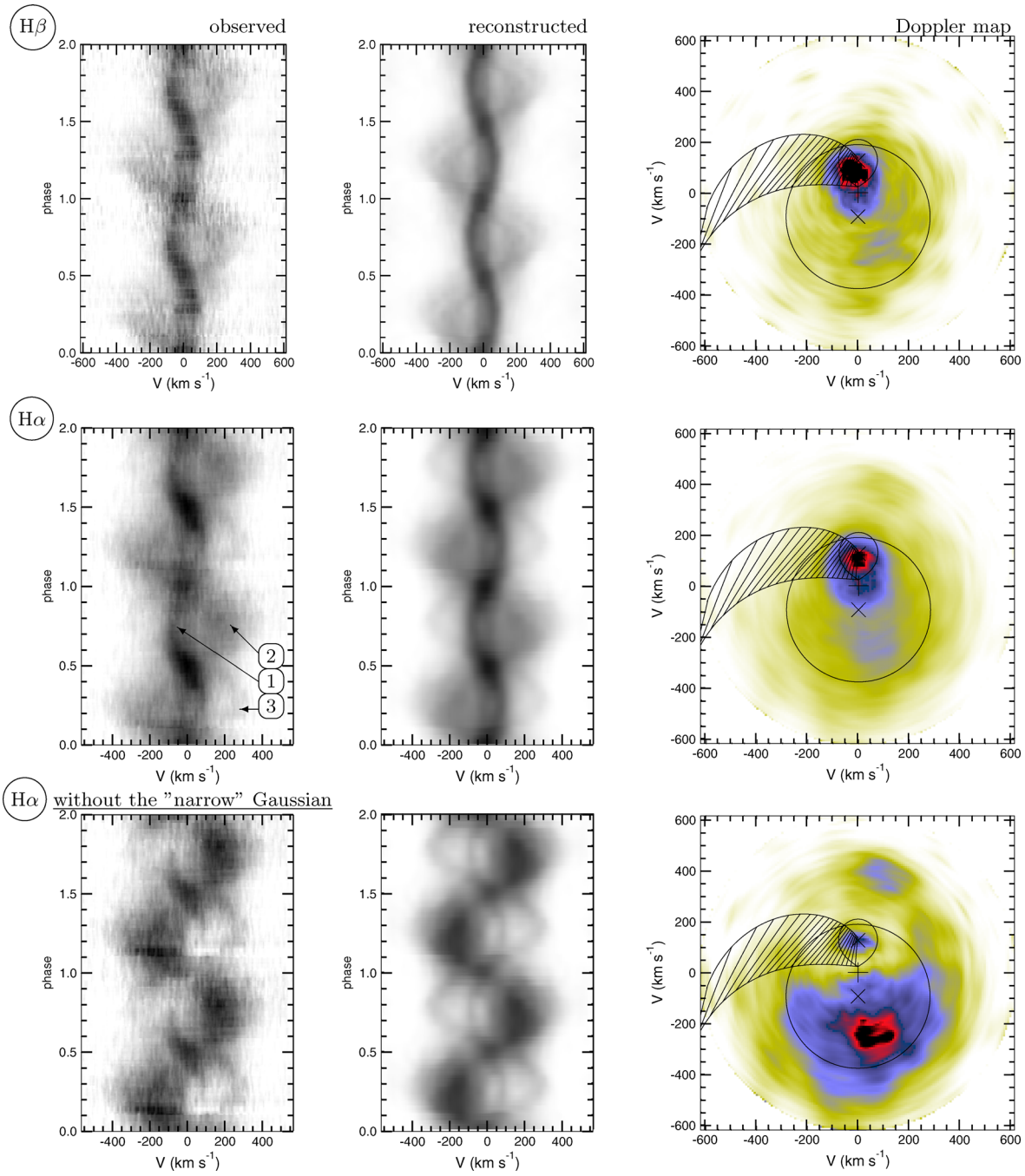

Figure 3. The observed and reconstructed trailed spectra and the corresponding Doppler maps (from left to right columns) of the H α and H β emission lines of RW Sex. The two upper rows show unaltered observed lines, while the bottom row shows the H α line after the subtraction of the 'narrow' emission component. Indicated on the maps are the positions of the Roche lobe of the secondary (upper bubble with cross), the centre of mass of the binary (middle plus symbol) and the WD (lower cross). The trajectory of the gas stream and the Keplerian velocity of the disc along the stream are also shown in the form of the lower and upper curves, respectively. The circle in the Doppler maps shows the tidal limitation radius r_d (max) of the accretion disc. All the marks are plotted for $M_1 = 0.84$ M$_\odot$, $i = 34^\circ$ and $q = 0.74$. The 'narrow', wide and third components of emission lines are denoted in one of the panels by respective numbers.

4.1 Eclipse modelling and system parameters of 1RXS J064434.5+334451

Light curves of 1RXS J064434.5+334451 in the *V* band and eclipse profiles in the *B*, *V* and *R* bands were presented by Sing et al. (2007, see their fig. 2) and Hernández Santisteban et al. (2017, see their figs 5 and 6). During the eclipse, the flux of the object decreases by about ∼1.25 mag and the spectrum slope changes from 'blue' to 'flat'. However, the Balmer emission lines do not diminish and they preserve their one-peaked shape (Sing et al. 2007, see their fig. 3).

The modelling technique developed by Zharikov et al. (2013) and Tovmassian et al. (2014) permits us to define the parameters of a binary system from an analysis of the eclipse light curve. Fig. 5 shows a geometrical model used for the fitting. It is composed of a concave accretion disc, a secondary star filling its Roche lobe, a stream from the inner Lagrangian point and a hotspot area of

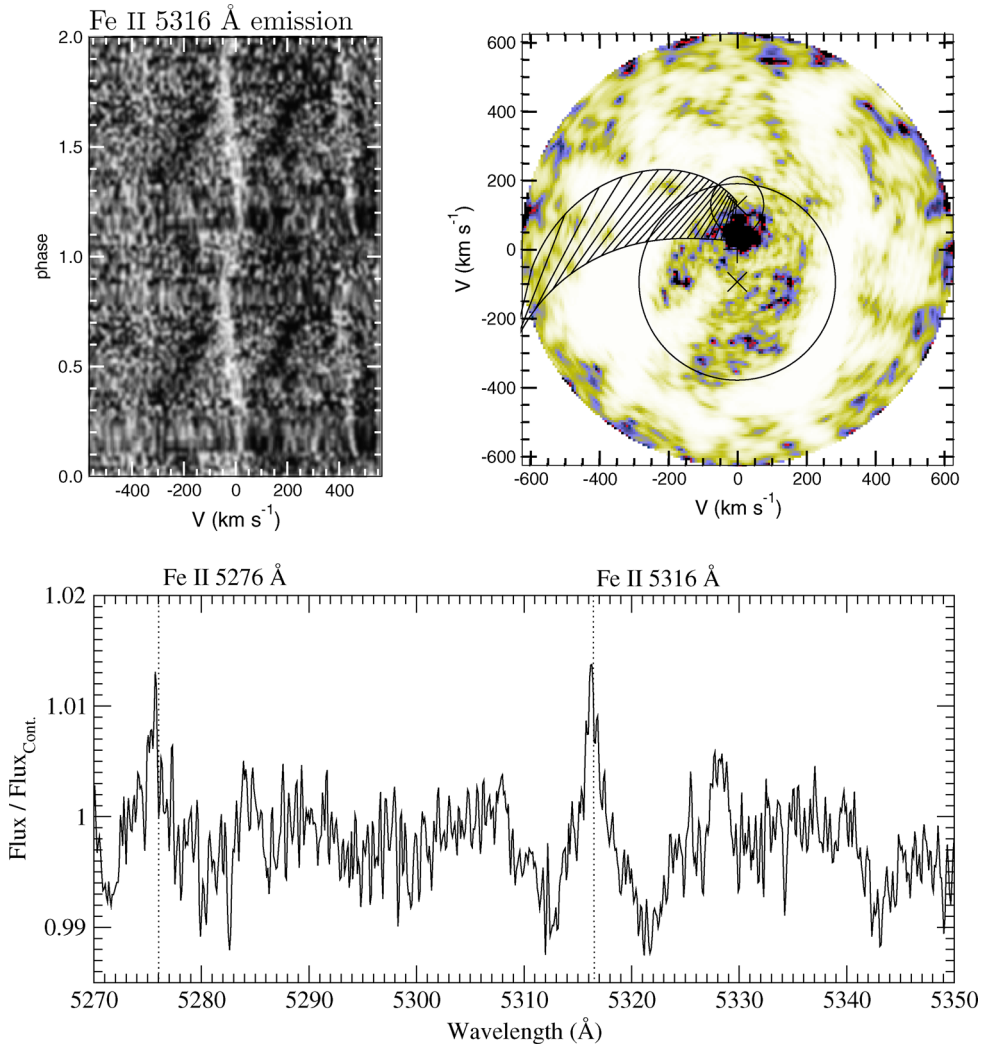

Figure 4. Bottom: the averaged spectrum of RW Sex in the 5270–5350 Å wavelength range, uncorrected for orbital motion. Top: the trailed spectrum of the Fe II 5316 Å line (left) and the corresponding Doppler map (right). The symbols on the Doppler map are overplotted in the same way as for Fig. 3.

Table 2. Parameters of the Gaussian components of the Hα emission core.

Emission component	$A \equiv V \sin(i)$ (km s^{-1})	V (km s^{-1})	I/I_c	FWHM (phase)	φ_0
RW Sex		$i = 34°$			
Narrow (1)	50.3	89.9	0.19	172.1	0.00
Wide (2)	164.6	294.4	0.14	484.4	0.43
1RXS J064434.5+334451		$i = 74°$			
Narrow (1)	68.6	71.4	0.22	216.6	0.00
Wide (2)	297.1	309.1	0.46	1379.9	0.42

interaction between the gas stream and the disc, which is located at the outer rim of the accretion disc. The concave accretion disc is characterized by the outer radius r_{out}, the opening angle h_{out}, as seen from the WD, and the slope γ_{disc}, controlling the vertical extension of the disc: $h = h_{out}(r/r_{out})^{\gamma_{disc}}$. The outer radius of the accretion disc r_{out} was fixed at the tidal truncation radius r_d(max) (equation 2). We assume that the disc radiates as a blackbody at the local temperature. The radial distribution across the disc is given by

$$T(r) = \left\{ \frac{3GM_1\dot{M}}{8\pi\sigma r^3} \times \left[1 - \left(\frac{R_1}{r} \right)^{1/2} \right] \right\}^{EXP}, \quad (3)$$

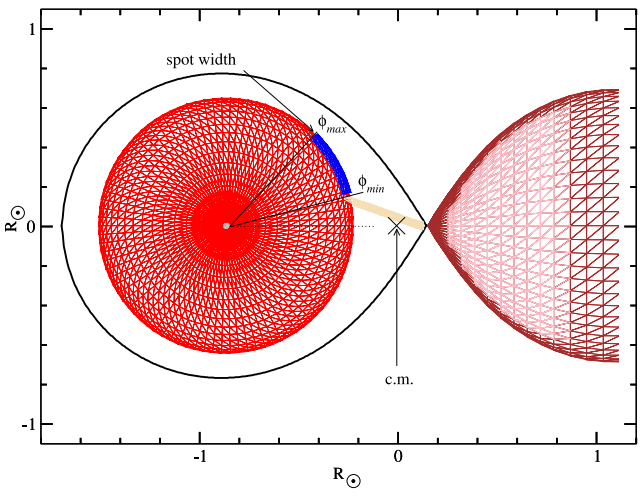

Figure 5. A schematic model of 1RXS J064434.5+334451. See description in the text.

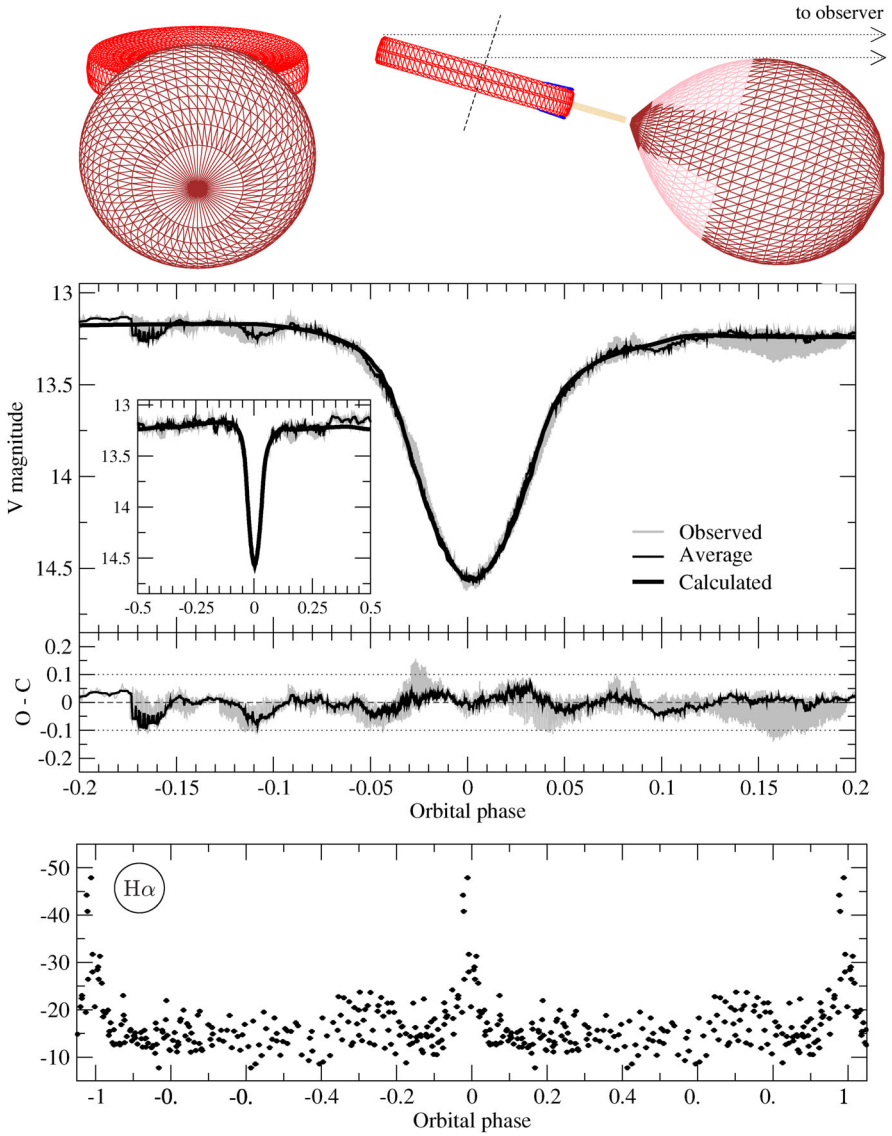

Figure 6. Top panel: a projection view of the 1RXS J064434.5+334451 model at orbital phases 0.0 (left) and 0.25 (right). Middle panel: the observed (averaged and individual) and best-fitting *V*-band eclipse profiles (top) and the corresponding residuals (bottom). Bottom panel: EW variation of the Hα emission line with orbital phase.

where M_1 and R_1 are the mass and the radius of the WD, respectively, $\dot{M}$ is the mass-transfer rate, G is the gravitation constant and σ is the Stefan–Boltzmann constant. The radial temperature gradient *EXP* in the standard accretion disc model is equal to 0.25 (Warner 1995, equation 2.35), but we allow it to slightly deviate from this value, following Linnell et al. (2010). The temperature of the WD corresponds to the temperature of the inner edge of the accretion disc $T_1 \equiv T_{\rm WD} = T_{\rm disc,\,in}$. We used the mass–radius relationship for WDs from Warner (1995, equation 2.82). The vertical extension and the temperature of the hotspot area linearly decline from maximum values $h_{\rm s,\,max}$ and $T_{\rm s,\,max}$ at the point $\phi_{\rm min}$ to minimum values $h_{\rm s,\,min} \equiv h_{\rm out}$ and $T_{\rm s,\,min} \equiv T_{\rm out}$ at $\phi_{\rm min}$, respectively (see Fig. 5).

The surface of each system component is divided into a series of triangles, and each triangle emits as a blackbody with the corresponding temperature. The total flux from the system is obtained by integrating the emission from all non-occulted elements lying in view, and then folded with the response of a photometric filter. Emission from the accretion stream is not taken into account. As a result, the code allows us to calculate the light curve of the binary in a selected photometric band and radial-velocity curves for all components (e.g. the primary or secondary star, the hotspot, etc).

To fit the eclipse profiles of 1RXS J064434.5+334451, we varied M_1, q, $\dot{M}$, *EXP*, $h_{\rm out}$, γ, the temperature of the secondary T_2 and the parameters of the hotspot with the aim to find the best coincidence

$$\sigma_{\rm min} = \sqrt{\frac{1}{N}\sum_{i=1}^{N}(O-C)^2} \qquad (4)$$

between the observed O and calculated C magnitudes in the $[-0.1;\ 0.1]$ range of orbital phases. The range was selected arbitrarily in order to exclude intrinsic disc variabilities (flickering), which is not periodic and is stronger out of the eclipse. However, we ensured that the flux outside the $[-\ 0.1;\ 0.1]$ interval does not exceed the observed.

The average *V*-band eclipse profile, the best fit and the residuals are plotted in Fig. 6. Individual eclipses, which were used to fetch

Table 3. Parameters of 1RXS J064434.5+334451 from the eclipse modelling. Numbers in parentheses are adopted uncertainties of the fit (see the text). $\mathrm{Width_{spot}}$ ($r_{\rm out}$) is fixed.

Parameter	Value
System	
M_1 ($\mathrm{M_\odot}$)	0.73(7)
M_2 ($\mathrm{M_\odot}$)	0.58
q	0.80(2)
i (°)	74.0(3)
T_2 (K)	4250(200)
R_1 ($\mathrm{R_\odot}$)	0.0105
R_2 ($\mathrm{R_\odot}$)	0.691
a ($\mathrm{R_\odot}$)	1.92
$\dot{M}$ ($\times 10^{-8}$ $\mathrm{M_\odot\ yr^{-1}}$)	0.15–1.5
Distance (pc)	390–800
Disc	
$r_{\rm out}/a$	0.33
$h_{\rm out}/r_{\rm out}$	0.15(5)
$\gamma_{\rm disc}$	1.0(5)
EXP	0.22(2)
Hotspot	
$\phi_{\rm min}$ (°)	12.4
$\phi_{\rm max}$ (°)	42.4(15)
$\mathrm{Width_{spot}}$ ($r_{\rm out}$)	0.05

the average profile and individual residuals, are also shown as a grey background. We allowed reasonable 10 per cent uncertainties to the fit because the scatter of magnitudes in the data is about 0.1 mag. The obtained parameters of the best fit are given in Table 3. The errors were obtained by a variation of each free parameter while fixing the others at their best values. The derived system parameters are close to those reported by Sing et al. (2007) and Echevarria (2015), and they are not consistent with those of Hernández Santisteban et al. (2017).

In particular, the radial-velocity semi-amplitude of the secondary star $K_2 = 191.6$ km s^{-1}, derived from our model, is in agreement with the value 192.8±5.6 km s^{-1} obtained from observations (Sing et al. 2007).

By adopting the best-fitting value of $\dot{M} = 0.8 \times 10^{-8}$ $\mathrm{M_\odot\ yr^{-1}}$, we determine the temperature of the outer edge of the accretion disc to be about 8500 K and ∼55 000 K for the inner parts of the disc. The hotspot is relatively compact, and its azimuthal extension is about 30°. The highest temperature in the spot is ∼10 500 K, only ∼2000 K hotter than the rest of the disc's edge. However, the maximal contribution of the hotspot to the total flux of the system in the *V* band is only about 10 per cent immediately before the eclipse. The contribution of the secondary star is insignificant during all orbital phases. Even at the minimum, its flux is at least five times lower than of the visible part of the disc.

The radial temperature gradient $EXP = 0.22$ is slightly smaller than the standard value 0.25. Models with $EXP = 0.25$ always give a narrower eclipse profile, producing deviations not only in the ingress and egress but also in the depth of the eclipse. We note that a similar deviation from the standard model was recently found for RW Sex by Linnell et al. (2010).

According to our model, the accretion disc is not totally eclipsed. The top panel of Fig. 6 shows the system from the observer's point of view at the zero orbital phase. The stream, the L_1 region, the WD and the central part of the disc around the primary are eclipsed completely. Only external parts of the accretion disc and space above $>0.2r_{\rm out}$ of the WD are unobscured. The temperature of the visible, inner part of the disc during the eclipse is below ∼20 000 K. While the brightness of the system falls over ∼ three times at the bottom of the eclipse, the emission in Balmer lines remains strong, resulting in an increase of equivalent widths (EWs), as can be seen from the lower panel of Fig. 6. From the system geometry and the appearance of the Hα line during the eclipse, we conclude that the Hα line forming region is located above or in the outermost parts, or beyond the accretion disc.

4.2 Emission-line components and Doppler tomography of 1RXS J064434.5+334451

We used the same method, described above, for the case of RW Sex, to separate the 'narrow' and the 'wide' components of Hα emission in 1RXS J064434.5+334451. The resulting parameters of the fit are presented in Table 2. In Fig. 7, we have reproduced the Hα Doppler map for the entire line (upper panels) as well as after subtraction of the 'narrow' component (bottom panels). The 'wide' component is concentrated in the lower-right quadrant of the tomogram at ($V_x \sim 200$ km s^{-1}, $V_y \sim -350$ km s^{-1}), but is extended from $V_x \sim -400$ to $+400$ km s^{-1} and from $V_y \sim -200$ to -500 km s^{-1}. These velocities are significantly lower than expected at the tidal truncation radius of the disc,[4] and thus the location of any emission structures here is unexpected. This could suggest that this region is also situated beyond the outer edge of the accretion disc.

Moreover, the values of radial velocities in Table 2 lead to a very important conclusion: the respective radial velocities ($RV_{\rm obs}$) of each component are a function of the inclination angle $A \equiv RV_{\rm obs} = V \sin(i)$. Applying the best-estimated inclination angles for each system, we obtain analogous velocities for both objects $V_{\rm narrow} \approx 80$ km s^{-1} and $V_{\rm wide} \approx 300$ km s^{-1}, respectively. The slightly spread of those values can be owned by the differences in component masses in the systems and ambiguity of inclination angle for RW Sex. This strongly supports the idea that the 'wide' component belongs to the orbital plane and does not originate in a wind perpendicular to the accretion disc.

5 ACCRETION FLOW STRUCTURE IN LONG-PERIOD NL SYSTEMS

It is widely accepted that NLs in a high state have a high mass-transfer rate. As a result, they have hot ($\gtrsim 10\,000$ K), optically thick accretion discs in an almost steady state, which are expected to produce broad absorption lines instead of emission lines, which is common among other CVs in quiescence. Nevertheless, we routinely observe emission features in many NLs. Usually, these emissions lines appear simply single-peaked in low-resolution spectra. However, the Balmer line profiles in the high-resolution spectra of two NL systems, RW Sex and 1RXS J064434.5+334451, are complex and comprised of an absorption component from the optically thick accretion disc, and of at least two emission components, labelled here as 'narrow' and 'wide'. The 'narrow' component with a low radial-velocity amplitude originates at L_1 and/or the irradiated surface of the secondary facing the disc. Meanwhile, the origin of the 'wide' component is not clear. We summarize its main features as follows.

(i) The radial velocity varies with the orbital period.
(ii) The orbital phase is shifted relative to the 'narrow' component by about 0.43 (rotated clockwise on the Doppler maps).

[4] For the adopted system parameters of 1RXS J064434.5+334451, the projected Keplerian velocity at the tidal truncation limit is ∼450 km s^{-1}.

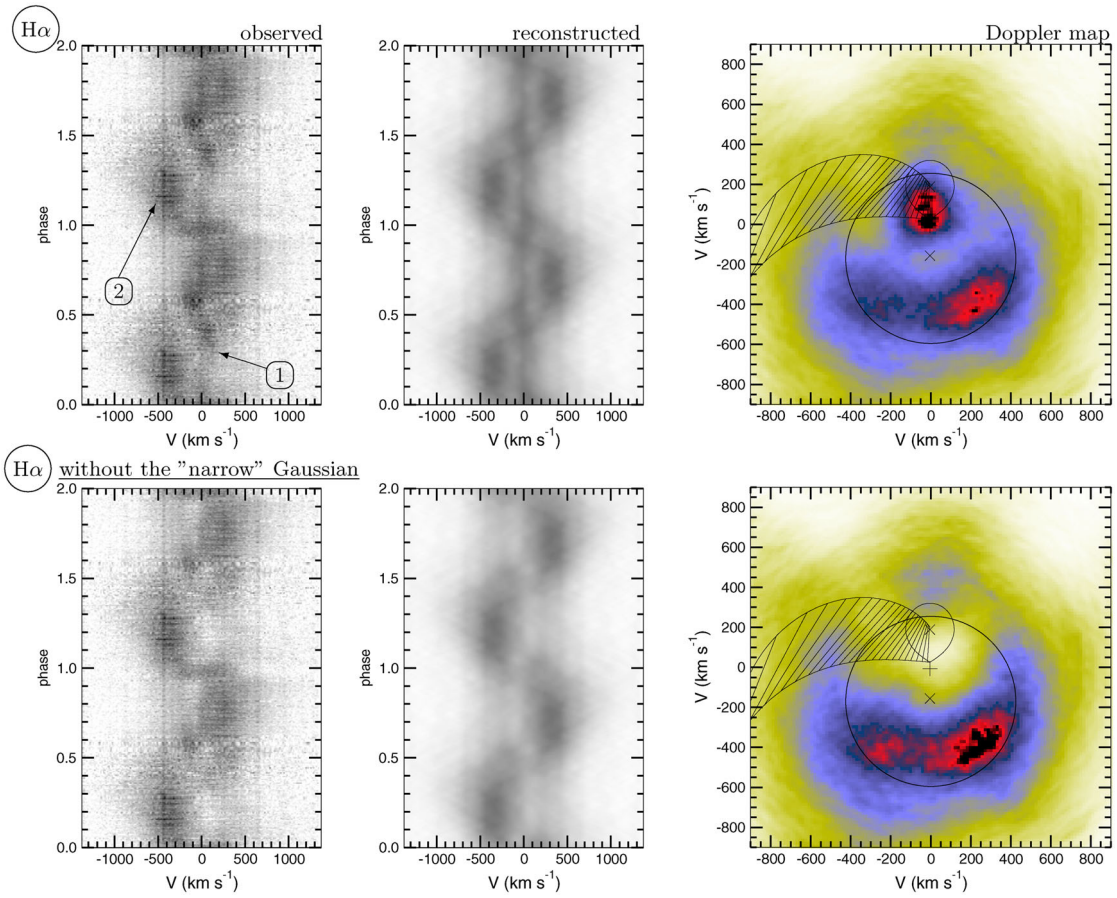

Figure 7. Observed and reconstructed trailed spectra and the corresponding Doppler maps (columns from left to right) of Hα of 1RXS J064434.5+334451. The top panels show the observed, unaltered line, while the bottom row shows Hα after the subtraction of the 'narrow' component. The 'narrow' and 'wide' components of Hα are marked on the observed trailed spectrum by '1' and '2', respectively. The symbols on the Doppler maps are plotted for $M_1 = 0.73$ M$_\odot$, $i = 74^\circ$, $q = 0.80$.

(iii) Unlike the He II line, the 'wide' component is not related to the WD (see the He II tomogram of 1RXS J064434.5+334451 in Hernández Santisteban et al. 2017).

(iv) The wide component does not disappear during eclipses.

(v) The spot created by the wide component on the Doppler maps appears to be identical for both the low- and high-inclination systems.

(vi) The shape and large size of that spot on the Doppler maps indicates strong velocity dispersion of the forming region.

In order to examine how unique such a structure is, we visually inspected the available Doppler maps and/or trailed spectra of non-magnetic NL systems with orbital periods longer than 4 h. Unfortunately, although the current edition of the Ritter & Kolb (2003) catalogue (update 7.24, 2016) lists more than 35 such NLs, only about a quarter of these were studied spectroscopically. However, we found that most of them are high-inclination eclipsing systems exhibiting, similarly to 1RXS J064434.5+334451, single-peaked Balmer, He I and occasionally He II emission lines in and out of eclipses (see, e.g. RW Tri, IX Vel, V347 Pup, V3885 Sgr, AC Cnc, V363 Aur and BF Eri; Kaitchuck, Schlegel & Honeycutt 1983; Kubiak, Pojmanski & Krzeminski 1999; Thoroughgood et al. 2004, 2005; Hartley et al. 2005; Neustroev & Zharikov 2008). Moreover, their Doppler maps and/or trailed spectra also show similarities to those presented in this paper, which allows us to propose a common behaviour of an accretion flow in long-period NLs.

In order to explain the presence of single-peaked emission line profiles in high-inclination CVs, several possible models have been suggested, such as Stark broadening (Lin, Williams & Stover 1988), magnetic accretion (Williams 1989), wind emission (Honeycutt, Schlegel & Kaitchuck 1986; Murray & Chiang 1996; Matthews et al. 2015), disc-overflow accretion (Hellier & Robinson 1994) and an extended bright spot as the dominant source of emission lines (Dhillon et al. 1997; Tovmassian et al. 2014).

The first three are related to the WD and/or the innermost part of the accretion disc. It is naturally expected that a source of emission lines in those models will demonstrate an orbital motion, which is related to the position of the WD and which we do not observe in the Balmer lines of RW Sex and 1RXS J064434.5+334451. In fact, a perpendicular wind in a high-inclination system such as the latter will produce an emission line with practically zero velocity. This phenomenon was observed during the super-outburst of V455 And (Tovmassian et al. 2011). The disc during the outburst becomes optically thick, similar to NLs. Meanwhile, emission lines are produced in the wind, converting a perfect ring depicting a quiescent accretion disc into a concentrated spot at the centre of Doppler maps throughout the super-outburst. In the case of RW Sex and 1RXS J064434.5+334451, we observe quite a different effect – the higher the inclination angle of the binary plane, the higher the velocity of the 'wide' component. Therefore, the matter, emitting the 'wide' component, is confined to the orbital plane, but not within the tidal truncation radius of the accretion disc.

The disc-overflow model predicts that a significant fraction of the stream can overflow the outer disc edge and hit the far, following side of the disc close to its circularization radius (Kunze, Speith & Hessman 2001). Neither the velocity coordinates nor the azimuthal coordinates of the 'wide' emission components are consistent with this prediction. The model of an extended bright spot was developed to explain unusual properties of the SW Sex stars. In this respect, we note that Hernández Santisteban et al. (2017) suggested that the characteristics of 1RXS J064434.5+334451 are consistent with an SW Sex star. However, although some similarities can indeed be found, we doubt this classification.

One of the defining properties of SW Sex objects is that in the eclipsing stars the emission-line radial-velocity curves show a substantial delay (∼0.2 orbital cycle) with respect to the motion of the WD. Such a behaviour can be understood by assuming that the primary source of emission lines in the SW Sex objects is the hotspot (Tovmassian et al. 2014). However, the contribution of the hotspot is negligible in both objects of this study and the phasing of the radial-velocity curve of 1RXS J064434.5+334451 agrees well with that expected from the eclipses (see fig. 9 in Hernández Santisteban et al. 2017). Also, the high-velocity (broad) emission components in both objects show maximum blueshift near phase 0.25 (Figs 3 and 7), whereas in the confirmed SW Sex stars maximum blueshift of high-velocity emission S-waves is observed near phase ∼0.5 (see, e.g. fig. 3 in Dhillon, Smith & Marsh 2013 and fig. 6 in Tovmassian et al. 2014). We believe that these differences are essential, and thus the suggestion of Hernández Santisteban et al. (2017) that 1RXS J064434.5+334451 is an SW Sex star is not valid.

Thus, neither of the models described above can explain the emission structure of RW Sex and 1RXS J064434.5+334451. However, Bisikalo et al. (1998) pointed out that in high-mass-transfer rate binaries, the matter can escape the accretion disc and create a halo around the disc. According to their three-dimensional gas-dynamical simulations of accretion flows in a 5.4-h system with typical stellar parameters and a mass-transfer rate of 10^{-8} $M_\odot$ yr^{-1}, an extended low-velocity region (hereafter called an 'outflow zone') is filled with matter pouring from the disc (Bisikalo et al. 2008; Kononov et al. 2012). This region is located practically on the opposite side of the disc with respect to the hotspot (labelled as A and B in fig. 3 in Bisikalo et al. 2008). In the synthetic Doppler map, the position of region B corresponds exactly to the large spot created by the 'wide' component of emission lines (Figs 3 and 7). The material in the outflow zone has a substantial velocity dispersion and hence does not form a concentrated spot. The outflow zone is not totally eclipsed even in a high-inclination system. Also, the material from this zone comes to form a circumbinary ring (Bisikalo 2009, 2010), evidence of which was found in some NLs (including RW Sex) in far-infrared observations (Hoard et al. 2014). Therefore, we suppose this region (the zone of outflow) to be a possible source of the 'wide' component of the Balmer line profiles in RW Sex and 1RXS J064434.5+334451, and possibly other long-period NLs. The same region was also recently proposed by Tovmassian et al. (2014) to be responsible for the appearance of absorption dips in the emission lines of SW Sex stars around phase 0.4–0.7.

The difference in the appearance of this region in SW Sex stars, the majority of which are found with orbital periods shorter than 4 h,[5] and long-period NLs is intriguing. We believe that the key is the mass-transfer rate. Indeed, according to standard evolutionary theory, the mass-transfer rate decreases during the CV evolution. Howell, Nelson & Rappaport (2001) showed, through population synthesis, that the mass-transfer rate in CVs with orbital periods of 3–4 h is about 5–10 times lower than in CVs with periods longer than ∼6 h. The immediate consequence is a substantially different temperature of the accretion disc in the longer and shorter orbital period systems (see, e.g. equation 3). Below, we give our qualitative view on the observational transformation of NLs during their evolution from longer to shorter orbital periods.

(i) In long-period systems with a high mass-transfer rate, the disc is hot, dense and optically thick. The outer edge of the disc reaches $\gtrsim$10 000 K and emits mainly in the continuum, producing broad absorption lines, like the atmosphere of a B- or A-type star. The hotspot contributes only modestly to the continuum emission because its material is dense, optically thick and the difference in temperature between the disc edge and the hotspot is relatively small. The emission lines are primarily formed outside the accretion disc, in the outflow zone ('wide' component) and on the surface of the secondary ('narrow' component). The objects observationally resemble RW Sex.

(ii) At shorter orbital periods, the mass-transfer rate diminishes and the temperature at the disc edge also drops below 10 000 K, while the disc generally remains hot and dense (steady-state regime). Less matter leaves the disc and the temperature at the outflow zone is much lower. Hence, the outflow zone ceases to produce emission lines. Instead, it manifests itself as transient absorption features at orbital phases around ∼0.5. The irradiation of the secondary is probably not sufficient enough to contribute to emission lines. Meanwhile, the difference in temperature between the disc edge and the hotspot increases and the latter becomes the dominant source of emission. Such an object is observed as an SW Sex star.

6 CONCLUSIONS

With the help of high-resolution spectroscopy, we clearly showed that the H α emission-line profiles in the spectra of two long-period (∼6 h) NL systems, RW Sex and 1RXS J064434.5+334451, have a complex structure consisting of at least two distinct, variable components. These emission components ('narrow' and 'wide') create identical structures in the Doppler maps of both objects. We also found hints of similar emission structures in other long-period NLs. The source of the narrow, low-velocity component is located on the surface of the secondary star facing the accretion disc, or near the L_1 point. The other, wide component is probably not related to the WD or the central parts of the accretion disc but emanates from the outer side of the disc. We propose that its source is an extended, low-velocity region in the outskirts of the accretion disc, on the opposite side with respect to the hotspot. This naturally explains the profiles of Balmer emission lines observed in long orbital period NLs in which both components can hardly be separated in low-resolution spectra.

ACKNOWLEDGEMENTS

This work is based upon observations carried out at the OAN SPM, Baja California, Mexico. GT and SZ acknowledge PAPIIT grants IN108316, IN100617 and CONACyT grant 166376. We are grateful to Dr J. V. Hernández Santisteban for the opportunity to work with the original data of 1RXS J064434.5+334451. We thank the daytime and night support staff at the OAN-SPM for facilitating and helping to obtain our observations.

[5] See D. W. Hoard's Big List of SW Sextantis Stars (Hoard et al. 2003), available at http://www.dwhoard.com/biglist.

REFERENCES

Beuermann K., Stasiewski U., Schwope A. D., 1992, A&A, 256, 433
Bisikalo D. V., 2009, in Zhelyazkov I., ed., AIP Conf. Ser. Vol. 1121. American Institute of Physics, New York, p. 3
Bisikalo D., 2010, in Prša A., Zejda M., eds, ASP Conf. Ser. Vol. 435, Binaries – Key to Comprehension of the Universe. Astron. Soc. Pac., San Francisco, p. 287
Bisikalo D. V., Boyarchuk A. A., Chechetkin V. M., Kuznetsov O. A., Molteni D., 1998, MNRAS, 300, 39
Bisikalo D. V., Kononov D. A., Kaigorodov P. V., Zhilkin A. G., Boyarchuk A. A., 2008, Astron. Rep., 52, 318
Coppejans D. L., Körding E. G., Miller-Jones J. C. A., Rupen M. P., Knigge C., Sivakoff G. R., Groot P. J., 2015, MNRAS, 451, 3801
Dhillon V. S., Marsh T. R., Jones D. H. P., 1997, MNRAS, 291, 694
Dhillon V. S., Smith D. A., Marsh T. R., 2013, MNRAS, 428, 3559
Echevarria J., 2015, IAU General Assembly, 22, 2258553
Greenstein J. L., Oke J. B., 1982, ApJ, 258, 209
Hartley L. E., Murray J. R., Drew J. E., Long K. S., 2005, MNRAS, 363, 285
Hellier C., Robinson E. L., 1994, ApJ, 431, L107
Hernández Santisteban J. V., 2012, Mem. Soc. Astron. Italiana, 83, 729
Hernández Santisteban J. V., Echevarría J., Michel R., Costero R., 2017, MNRAS, 464, 104
Hoard D. W., Szkody P., Froning C. S., Long K. S., Knigge C., 2003, AJ, 126, 2473
Hoard D. W. et al., 2014, ApJ, 786, 68
Honeycutt R. K., Schlegel E. M., Kaitchuck R. H., 1986, ApJ, 302, 388
Howell S. B., Nelson L. A., Rappaport S., 2001, ApJ, 550, 897
Kaitchuck R. H., Schlegel E. M., Honeycutt R. K., 1983, ApJ, 267, 239
Kononov D. A., Giovannelli F., Bruni I., Bisikalo D. V., 2012, A&A, 538, A94
Kubiak M., Pojmanski G., Krzeminski W., 1999, AcA, 49, 73
Kunze S., Speith R., Hessman F. V., 2001, MNRAS, 322, 499
Levine S., Chakarabarty D., 1995, IA-UNAM Technical Report MU-94-04
Lin D. N. C., Williams R. E., Stover R. J., 1988, ApJ, 327, 234
Linnell A. P., Godon P., Hubeny I., Sion E. M., Szkody P., 2010, ApJ, 719, 271
Lynden-Bell D., 1969, Nature, 223, 690
Marsh T. R., Horne K., 1988, MNRAS, 235, 269
Matsuda T., Sekino N., Shima E., Sawada K., Spruit H., 1990, A&A, 235, 211
Matthews J. H., Knigge C., Long K. S., Sim S. A., Higginbottom N., 2015, MNRAS, 450, 3331
Murray N., Chiang J., 1996, Nature, 382, 789
Neustroev V. V., Zharikov S., 2008, MNRAS, 386, 1366
Neustroev V. V. et al., 2017, MNRAS, 467, 597
Noebauer U. M., Long K. S., Sim S. A., Knigge C., 2010, ApJ, 719, 1932
Perryman M. A. C., Lindegren L., Kovalevsky J., Hoeg E., Bastian U., 1997, A&A, 323, L49
Prinja R. K., Long K. S., Froning C. S., Knigge C., Witherick D. K., Clark J. S., Ringwald F. A., 2003, MNRAS, 340, 551
Ritter H., Kolb U., 2003, A&A, 404, 301
Sing D. K., Green E. M., Howell S. B., Holberg J. B., Lopez-Morales M., Shaw J. S., Schmidt G. D., 2007, A&A, 474, 951
Steeghs D., 2001, in Boffin H. M. J., Steeghs D., Cuypers J., eds, Lecture Notes in Physics Vol. 573, Astrotomography, Indirect Imaging Methods in Observational Astronomy. Springer, Berlin, p. 45
Thoroughgood T. D., Dhillon V. S., Watson C. A., Buckley D. A. H., Steeghs D., Stevenson M. J., 2004, MNRAS, 353, 1135
Thoroughgood T. D. et al., 2005, MNRAS, 357, 881
Thorstensen J. R., Davis M. K., Ringwald F. A., 1991, AJ, 102, 683
Tovmassian G., Gänsicke B., Zharikov S., Ramirez A., Diaz M., 2011, in Romero G. E., Sunyaev R. A., Belloni T., eds, Proc. IAU Symp. Vol. 275, Jets at All Scales. Kluwer, Dordrecht, p. 311
Tovmassian G., Stephania Hernandez M., González-Buitrago D., Zharikov S., García-Díaz M. T., 2014, AJ, 147, 68
Vitello P., Shlosman I., 1993, ApJ, 410, 815
Warner B., 1995, Cataclysmic Variable Stars, Cambridge Astrophysics Series Vol. 28. Cambridge Univ. Press, Cambridge
Williams R. E., 1989, AJ, 97, 1752
Woźniak P. R. et al., 2004, AJ, 127, 2436
Zharikov S., Tovmassian G., Aviles A., Michel R., Gonzalez-Buitrago D., García-Díaz M. T., 2013, A&A, 549, A77

This paper has been typeset from a TEX/LATEX file prepared by the author.